Resource-Efficient Technologies 4 (2018) 1–13

Resource-Efficient Technologies

journal homepage: http://reffit.tech/index.php/res-eff

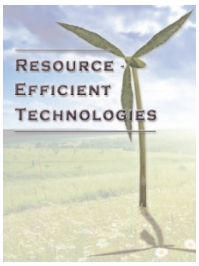

Research Paper

DYNAMIC BEHAVIOR PREDICTION OF LITHIUM POLYMER BATTERY FOR LOW-POWER SOLAR PV APPLICATIONS

A. K. Rohit*, S. Rangnekar

Energy Centre, Maulana Azad National Institute of Technology, Link Road Number 3, Near Kali Mata Mandir, Bhopal, Madhya Pradesh, India 462003

Abstract

With an increase in the amount of renewable, solar photovoltaic in particular, developing efficient energy storage media will become increasingly important. Batteries are one of the most common storage devices, and the maximum runtime and dynamic behavior of batteries play an important role in various energy storage applications. Therefore, it is crucial to understand the battery behavior during charging and discharging operation. This study aims to analyze the properties of a lithium polymer battery to support low-power Solar PV applications through experiment and simulation with a goal of understanding its electrical behavior. A simple experimental test procedure was used to determine the various electric parameters required to develop a model of the battery. Simulations results at various C rates captured the dynamic behavior of the lithium polymer battery, revealing an acceptable trade-off between accuracy and complexity.

Key words: lithium polymer battery, pulse discharge test, battery characteristics, state of charge, solar PV module, dynamic behavior of battery.

1. Introduction

The production and distribution of energy using a wide variety of sources has long been an inseparable part of human life. The significant increase in the global energy demand over the past few decades [1] has been accompanied by the concerns over environmental degradation from emissions and a growing interest in the development of the alternative energy sources that can displace the use of fossil fuels [2]. The clean energy production profiles of the renewable energy sources make them the best alternative and substitute for the fossil fuels in the coming years [3].

Among the renewable sources, solar photovoltaic energy generation has become crucial because it is easy to install and solar radiation is available year-round in most countries. Solar PV can provide electricity even at remote locations where the grid is not accessible in the form of standalone systems. However, the full utilization of Solar PV is hindered by recurrency factors such as the unavailability of solar power during the night [4]. Accordingly, energy storage has become an essential component of Solar PV systems as a means of storing energy during the daytime for subsequent on-demand use.

* Corresponding author. Energy Centre, Maulana Azad National Institute of Technology, Link Road Number 3, Near Kali Mata Mandir, Bhopal, Madhya Pradesh, India 462003. E-mail address: amitrohit8@gmail.com

Peer review under responsibility of Tomsk Polytechnic University.

https://doi.org/10.18799/24056537/2018/4/213

Currently, there are a number of available energy storage technology options, among which battery energy storage is the most widely used and commercially available. Batteries are used in numerous applications, such as electric and hybrid vehicles [5–8] and renewable energy systems [8–11], among others. Batteries serve as standby facilities in wind and solar photovoltaic systems by storing excess generated energy for release during the demand and at night, respectively [9, 10]. Battery energy storage is becoming the most flexible option for use in rural standalone systems because it is a technology that has been in use for long enough that most of its initial faults and inherent problems have been removed or reduced by further development, the most readily available and is portable. Such systems can also be scaled up on demand [4]. Batteries are widely used as energy storage and power sources in numerous electrical systems and devices, and the increased use of portable electronics in numerous applications has driven the growth of battery technologies such as nickel cadmium (NiCd), nickel–metal hydride (NiMH), lithium-ion (Li-ion), and Li-ion polymer to meet the advanced energy demands and size restrictions of current portable electronics [12].

Despite these advances, lead acid batteries remain the most commonly used battery storage technology in PV systems. Such batteries have disadvantages in terms of lower lifetimes and efficiencies, heavy, lower energy and power densities, higher self-discharge rates, and negative environmental effects when they are disposed [4, 13]. There are a number of emerging battery technologies for use in renewable storage that can overcome these limitations. Lithium polymer batteries [4, 14], for example, have a number of advantages over lead acid batteries, including higher cycle efficiencies, low self-discharge, high energy and power densities, and reduced environment impact [4]. These benefits make lithium batteries a good candidate for use in PV applications. The accurate modeling and simulation of battery performance is important in successfully integrating such devices into various applications including Solar PV systems [15].

In this study, a lithium polymer battery for use in low-power Solar PV systems was modeled and its performance was simulated. A simple and quick experimental test procedure was applied to determine the parameters required for precise modeling of the dynamic characteristics of the battery. The resulting model could accurately compute the State-of-Charge (SOC) value throughout the runtime. Simulation was then conducted at various C rates to predict the dynamic behavior of the battery, and the simulation results were validated using experimental data.

2. Solar PV module and lithium polymer battery specifications

A $50W_p$ Solar PV module was used as the power generation source in this study. The ratings of the PV module are listed in Table 1 below.

Table 1. *Technical specifications of Solar PV module.*

Parameters	Value
Open circuit voltage (*Voc*)	21.0 V
Short circuit current (*Isc*)	3.15 A
Voltage at maximum power (V_{mp})	17.0 V
Current at maximum power (I_{mp})	2.95 A
Maximum power (P_{max})	50 W_p

A lithium polymer (Li-po) battery with a nominal capacity of 5.2 Ah was used as the experimental storage device, the primary technical specifications of the battery are listed in Table 2 [16]. The Li-po battery has a nominal voltage of 11.1 V, a nominal capacity of 5.2 Ah, a maximum discharge current of 10C (50 A), minimum cut-off voltage (V_{min}) of 10.5 V, and a maximum cut-off voltage (V_{max}) of 12.30 V during discharging and charging. A lamp load and rheostat were used as a load for battery discharging purposes.

Table 2. *Technical specifications of lithium polymer battery.*

Battery parameters	Value
Capacity C (Ah)	5.2 Ah
Nominal voltage (V)	11.1 V
Maximum battery voltage (V_{max})	12.6 V
Minimum battery voltage (V_{min})	10.3 V
Maximum continuous charge current	2 C
Maximum continuous discharge current	10 C

3. Modeling

3.1. Solar PV

There are several circuit-modeling approaches that can be used to extract PV module parameters. It is well understood from the literature that any PV device can be represented by an equivalent electric circuit [15]. The equivalent circuit for the PV system analyzed in this study is a one-diode model comprising a solar intensity-dependent current source, a p–n junction diode, and two resistances (R_s and R_{sh}/R_p), as shown in Fig. 1. Here, the resistance captures the dissipative effects and manufacturing defects that produce parasitic currents within the PV module [17].

In most practical cases, the shunt resistance is quite high and is often neglected during the analysis [18]. A mathematical model of a solar PV module can therefore be easily derived as follows [17]:

$$I_{ph} = [I_{scr} + (K_i (T_{aK} - T_{rK}))]\left(\frac{s}{S_r}\right), \quad (1)$$

$$I_{rs} = I_{scr}\left[\frac{I_{scr}}{[e^{(qV_{oc}/kN_sA_iT_{rK})}-1]}\right], \quad (2)$$

$$I_0 = I_{rs}\left(\frac{T_{aK}}{T_{rK}}\right)^3 e^{\left\{\frac{\left[(E_g q)\left(\frac{1}{T_{rK}}-\frac{1}{T_{aK}}\right)\right]}{k^* A_i}\right\}}, \quad (3)$$

$$I_{pv} = N_p I_{ph} - N_p I_0\{e^{[q(V_{pv}+I_{pv}R_s)/kN_sA_iT_{aK}]}-1\} - V_{pv} + \frac{I_{pv}R_s}{R_{sh}}, \quad (4)$$

where Equations (1)–(4) calculate the photo-generated current (I_{ph}), module reverse saturation current (I_{rs}), module saturation current (I_o), and total output current of the module (I_{pv}), respectively. As mentioned above, a 50W$_p$ solar PV module with the ratings listed in Table 1 was used in this study.

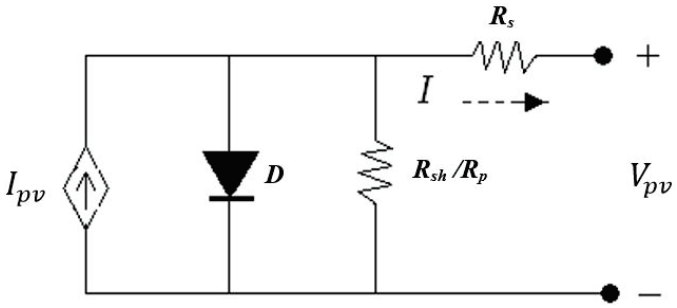

Fig. 1. *Electrical equivalent circuit of solar cell*

The output voltage of a PV module can be quite high and varies with the weather condition and therefore is not suitable for effective battery charging. Accordingly, a dc–dc buck converter, which steps down higher PV module input voltages to lower output voltages for charging the battery, is used as an interface between the PV module and battery.

3.2. DC–DC Converter

An electrical equivalent circuit of the buck converter is shown in Fig. 2. In this circuit, the switch (S) and diode (D) are considered to be ideal and R_L is considered to be the equivalent resistance of the inductor. Various types of switches can be used, including BJT, IGBT, power MOSFET, among others [18].

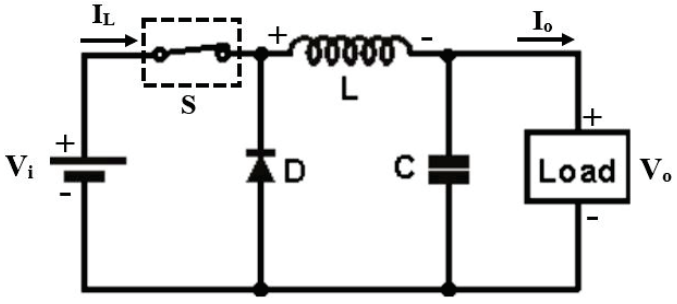

Fig. 2*. Electrical equivalent circuit of dc–dc buck converter*

The output voltage (V_{co}) of a buck converter is always less than the input voltage (V_s) and is given by

$$V_{co} = \alpha V_s, \quad (5)$$

$$V_{co} = \left(\frac{T_{on}}{T_{on}+T_{off}}\right)V_s. \quad (6)$$

The term in parentheses in Equation (6) is the duty cycle of the converter

$$\alpha = \frac{T_{on}}{T_{on}+T_{off}} = \frac{T_{on}}{T_s}, \quad (7)$$

where T_{on} and T_{off} are the on and off durations of the switch, respectively, and T_s is the duration of the switching time. Since the duty cycle is equal to the ratio of T_{on} to T_s, the value of varies between 0 and 1 (corresponding to T_{on}=0 to T_{on}=T_s, respectively).

Rearranging Equation (5) gives

$$\frac{V_{co}}{V_s} = \alpha, \quad (8)$$

which is the voltage gain of the buck converter. From Equation (8), it can be seen that at a given voltage the output voltage of the converter varies linearly with the duty cycle, which implies that the output voltage can be adjusted to a specific constant level by changing the duty cycle.

3.3. Lithium polymer battery

An equivalent circuit battery model that could be rapidly configured was used to simulate the performance of a lithium polymer battery with a streamlined configuration. Due to the dependence of the terminal voltage (V_t) of the battery on its open circuit or no load, voltage (V_{oc1}) can be easily obtained by calculating the results of a mathematical function during runtime. Thus, the model combines an electrical equivalent circuit with a mathematical component based on the battery's SOC.

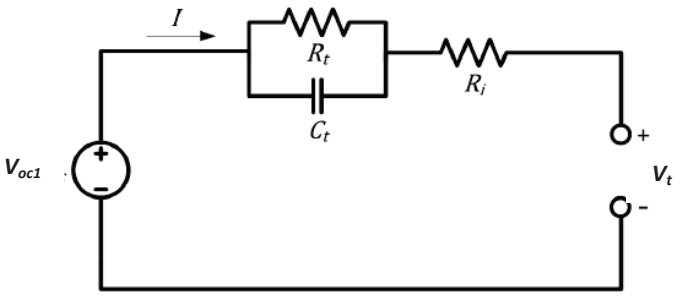

Fig. 3. *Electrical equivalent circuit of battery with single RC branch*

Although a battery can be represented using a linear model containing a single resistor to simulate its internal resistance [19], a Thevenin equivalent circuit was applied to obtain an accurate and clear representation of transient conditions in a simplified manner [16]. This model adds a parallel R_t, C_t block (R_t//C_t) in series with the internal resistance R_i. Although the accuracy and complexity of the model increases with

the number of RC networks, a single network can be used without significant sacrifice of simulation performance. Applying Kirchhoff's Voltage Law to the equivalent battery circuit in Figure 3 gives the following expression:

$$V_{oc1} = V_t + (R_i + R_t)I - R_t Ie^{\left(\frac{-t}{R_t C_t}\right)}. \quad (9)$$

4. Experimental setup and procedure

Charging and discharging tests were conducted at a constant current to determine the battery capacity.

4.1. Determination of battery capacity

The lithium polymer battery was charged at a current corresponding to an initial 1C rate up to the maximum cut-off voltage of 12.3 V, with the process continuing until the charging current was reduced to 10 % of its initial value, indicating that the battery capacity had been reached. From its completely charged state, it was easier to estimate the capacity C (Ah) of the battery by applying Equation (10) to the results of a discharge test at constant current I_b. Finally, the battery was discharged at constant current across a lamp load until the voltage reached its minimum cut-off value of 10.5 V (Fig. 6).

$$C = \frac{\int I_b \cdot dt}{3600}. \quad (10)$$

Following experimental measurement of the Li-po battery capacity, further tests were conducted to obtain various parameters.

All the above mentioned model parameters can be represented as multivariable functions of the states of charge, current, temperature, and recharge cycle number. Some battery parameters with negligible effects can be ignored, reducing the complexity of the system [16, 19]. For instance, the effect of temperature on battery capacity is minimal because low power applications undergo only minor temperature fluctuations at constant room temperature. As a result, the parameters can generally be expressed in terms of the SOC alone, resulting in a model that suitably trades off between accuracy and complexity, enabling experimental investigation that does not require complicated software or hardware tools. The test arrangement used in this study is shown in Fig. 4.

4.2. Test procedure

Discharge testing at a number of current steps was conducted to identify the model parameters using a hardware system built with the help of the LabVIEW data acquisition feature [20]. A block diagram and an image showing the hardware setup are shown in Fig. 4.

The battery was completely charged following the procedure described in the capacity determination section above and then discharged in a stepwise manner by supplying current at various levels to the load to reach different battery SOCs. At the end of each step, the discharge load was disconnected and the battery voltage was measured to obtain the instantaneous open circuit voltage (V_{io}). Following a pause to allow the circuit to reach equilibrium, voltage was again measured to obtain the open circuit voltage in equilibrium (V_{OE}) (Fig. 5).

As the capacity of the battery was 5.2 Ah, discharging it with a 5 A load for 38 seconds would consume 1 % of the total capacity, while discharging at 5A for 6 mins would consume ~10 % of the maximum available charge. Thus, the experimentally applied C rate of 0.9 C in steps of 6 mins consumed 10 % of the initial SOC per discharge. Following rest periods of 6 mins, during which no load was applied to the battery, the open circuit voltage was measured again to obtain values of V_{OE} that represented the battery terminal voltage with the circuit disconnected and the transient response extinct. Thus, each step period took 12 mins, with 6 mins of discharge and rest a piece. The measurements over an initial 6 mins provided adequate information and made the experimental procedure quick and simple to carry out [16].

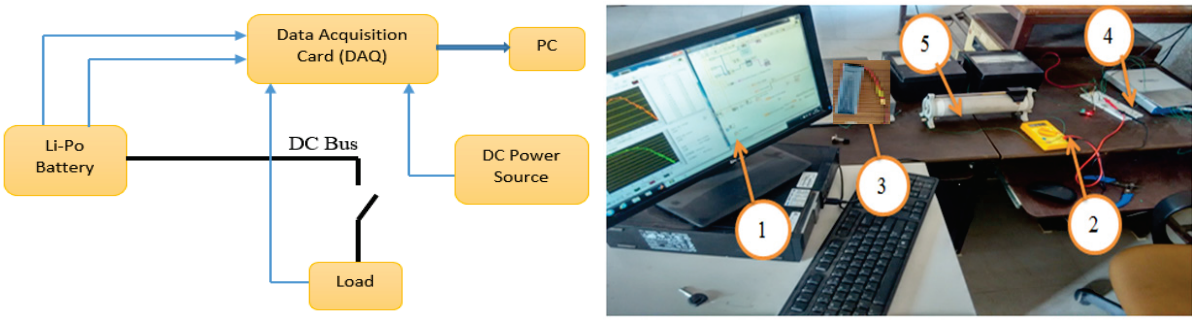

a) *b)*

Fig. 4. *a) Block diagram of experimental setup. b) Photo of setup: 1 – LabView; 2 – Multimeter; 3 – Li-po battery; 4 – DAQ Card; 5 – Load*

4.3. Internal resistance of battery (R_i)

A sudden voltage drop arising from the battery's internal resistance R_i appears the instant the battery is connected to a load. This internal resistance can therefore be calculated by dividing the difference between the open circuit voltage and the voltage under load by the load current:

$$R_i = \left(\frac{V_{oc1} - V_1}{I} \right), \tag{11}$$

where V_{oc} is the initial voltage of the battery and V_1 is the terminal voltage just after the load goes online. The values of R_t and C_t can also be calculated in terms of the length of time needed by the battery to reach its equilibrium potential, i.e., the relaxation period, once the load has been removed. By including the time constant (τ), the effects of the diffusion process and charge transfer between the electrodes and electrolyte can be incorporated into the model:

$$\tau = R_t C_t, \tag{12}$$

where

$$R_t = \left(\frac{V_{oc1} - V_t'}{I} \right). \tag{13}$$

4.4. Determination of the Open-circuit voltage (V_{oc}) and SOC

Measuring the open circuit voltage during runtime is impossible as, by definition, V_{oc} can only be measured if the battery is under an open circuit or no load condition. To overcome this limitation, it is necessary to evaluate the SOC of the battery. The per-unit SOC can be determined during the discharge period from the initial per-unit state-of-charge SOC_{int} as follows:

$$SOC(t) = SOC_{int} - \left(\frac{C(Ah)}{C_{\max}} \right). \tag{14}$$

Equation (14) can then be substituted into Equation (10) to obtain

$$SOC(t) = SOC_{int} - \left[\frac{1}{C_{\max}} \left(\frac{\int I_b \cdot dt}{3600} \right) \right]. \tag{15}$$

Thus, by measuring the amount of charge stored or released (charging or discharging) at any instant during runtime, i.e., using the coulomb counting method, the SOC of the battery at any instant can be calculated as shown in Fig. 5.

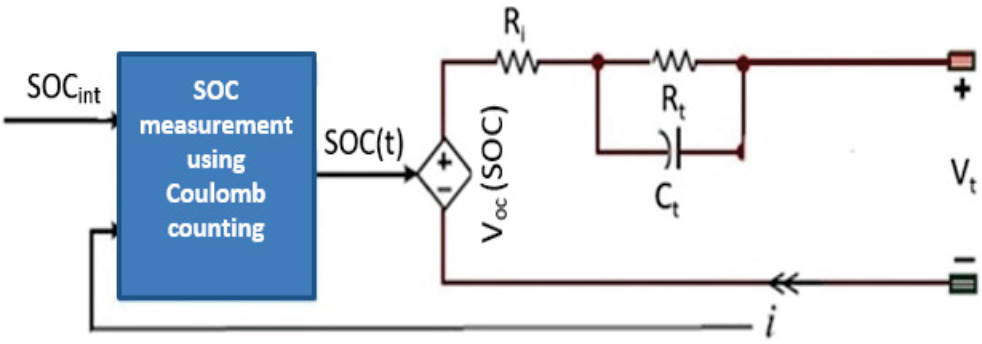

Fig. 5. *Battery model*

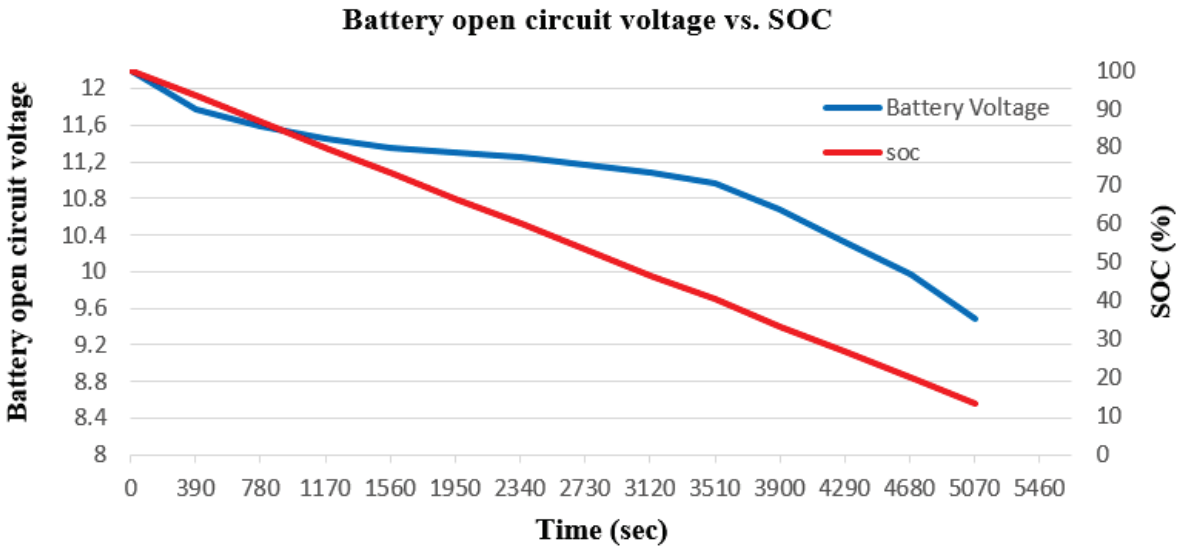

Fig. 6. *Pulse discharge test results*

4.5. Open circuit voltage estimation

In general, V_{oc1} is a function of the battery SOC and operating temperature [21]. To remove the effects of environmental temperature on the battery operation results produced in this study, all experiments were performed at room temperature and under environmental conditions.

As detailed in the preceding sections, the battery was repeatedly discharged in steps of 10 % of SOC and the voltage at the end of each rest period was measured. The experimental data obtained from these pulse discharge tests were plotted (Fig. 6) and a mathematical relation was obtained using a curve-fitting technique to estimate the battery $V_{oc1}(t)=f[SOC(t)]$ as the following exponential function of SOC:

$$V_{oc1}(SOC) = -1e^{15\,SoC} + 0.785SoC^3 - \\ -0.99SoC^2 + 0.125SoC + 11.42. \quad (16)$$

5. Matlab models

This section presents the Matlab Simulink models used to simulate the PV and battery systems, which were developed using the equations and experimentally determined parameters discussed in the preceding sections.

5.1. Solar PV Model

The Matlab Simulink model used to obtain the output characteristics of the 50 W_p Solar PV module is shown in Fig. 7. As both solar radiation and temperature affect the output of the PV module, simulation was carried out at various temperatures and solar radiation levels. The output characteristics are shown in Fig. 8.

Changes in solar irradiation with weather condition will cause the PV module output to fluctuate, but control mechanisms can be used to track such changes and allow for the extraction of sufficient power to meet the required load demand. At a given voltage value, increases in the solar irradiance will increase both the output power and current of the module. This occurs because the incidence of additional sunlight on the solar cell imparts a higher excitation energy to the cell's carrier electrons, which in turn generate more output power.

5.2. DC–DC buck converter model

Figure 9 shows the Matlab model of the dc–dc buck converter. Ports 1 and 2 are inputs into which the Solar PV module output is fed, while ports 3 and 4 produce a constant output voltage. A closed voltage control loop is applied to this process using a proportional integral controller. Depending on the error signal, a pulse width modulation (PWM) signal with a varying duty cycle is generated to switch the MOSFET at high frequencies and maintain the output voltage at a level close to the reference voltage of 12.5 V.

Figure 10 shows the output of the buck converter at a constant input voltage with varying waveforms. It is that the converter steps down the 20 V source voltage (V_s) input from the solar PV module to a constant (V_{co}) 12.5 V at its output port. In doing so, the converter continuously checks the error signal and generates a PWM to maintain the pre-set output voltage for charging the Li-po battery.

5.3. Lithium polymer battery model

To predict the SOC and dynamic behavior of the lithium polymer battery while charging and discharg-

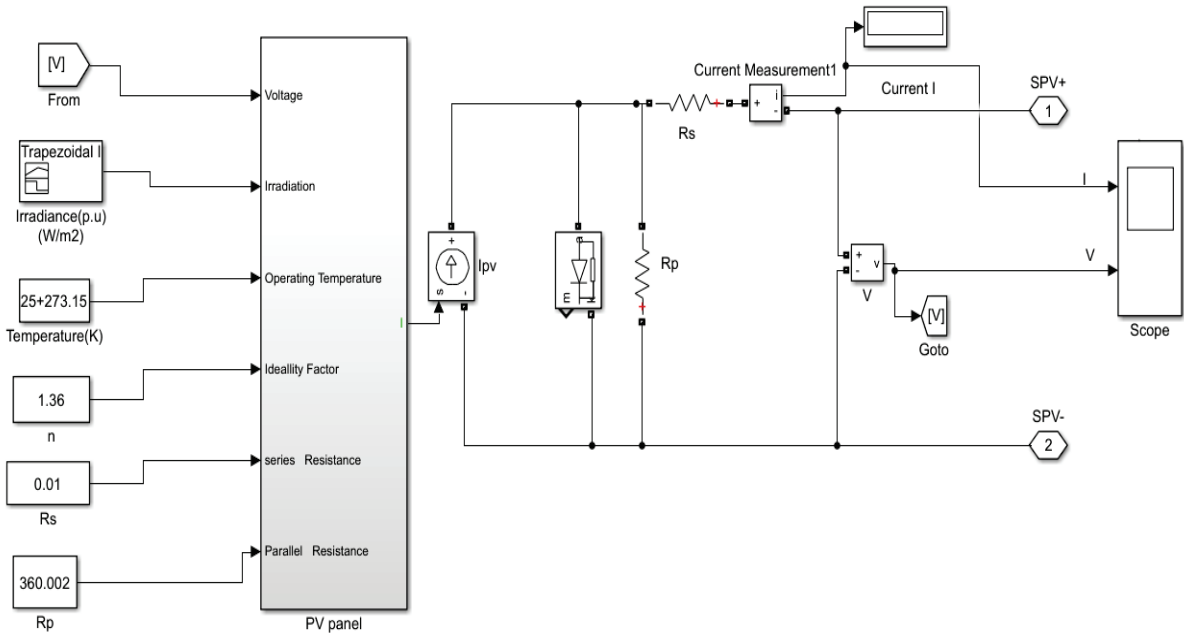

Fig. 7. *Matlab Simulink model of Solar PV module*

ing at various C rates, a Simulink model was constructed using the experimentally calculated parameters presented in the preceding sections. Figure 11 shows the lithium polymer battery model, where the input ports are connected to the output of the converter. The model continuously calculates the SOC of the battery, which varies between zero and one depending on the charging and discharging current. To protect the battery from overcharging and overdischarging, the model is able to monitor the SOC.

The instantaneous SOC of the model is obtained using coulometric measurement during runtime. Based on this SOC value, a mathematical function block computes the open circuit voltage using Equation (16), which is then simultaneously fed to the controlled voltage source. In this manner, the model is capable of precisely generating a battery terminal voltage, as shown in Figs. 12–13, which represents the terminal voltage characteristics of an actual PV system lithium polymer battery.

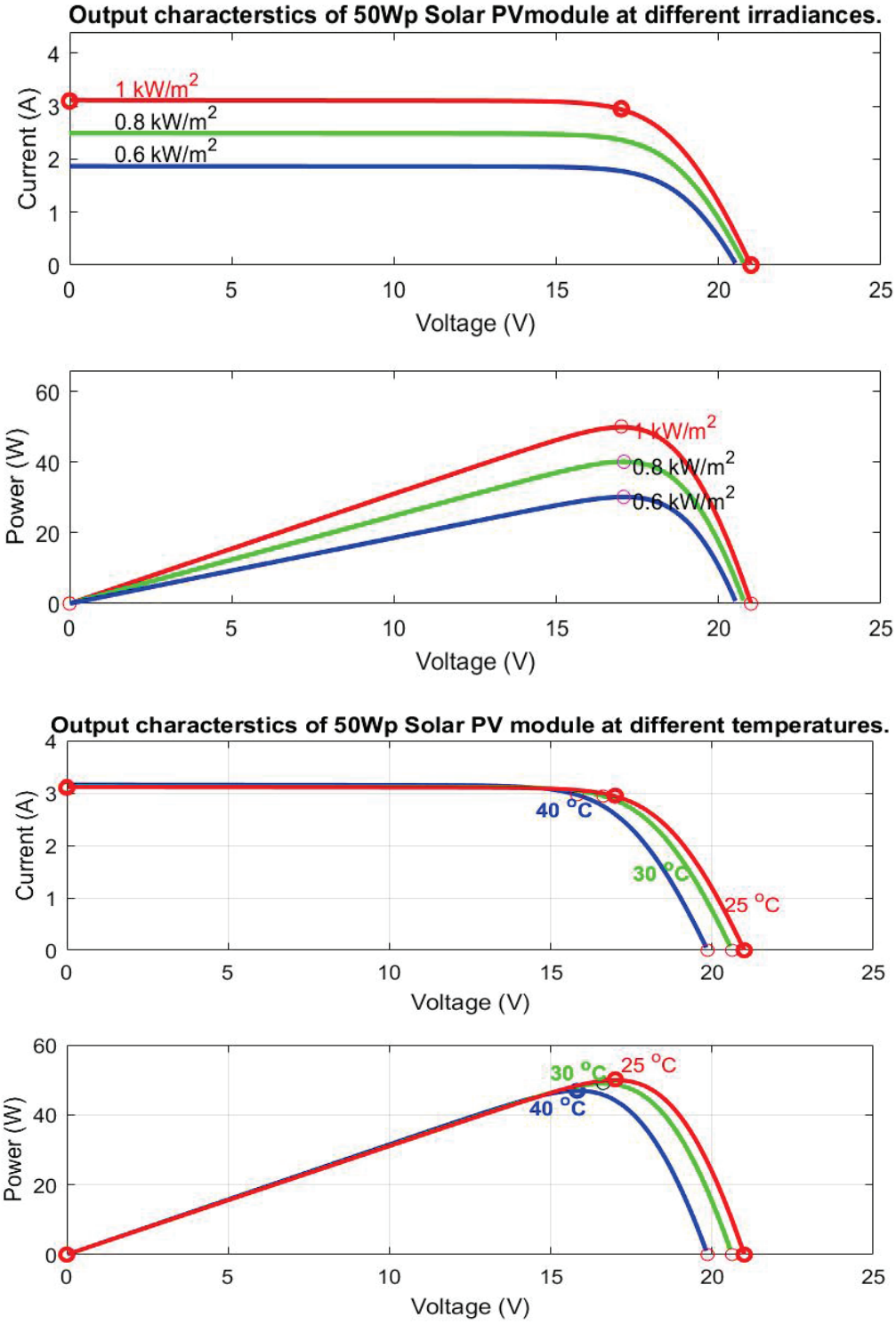

Fig. 8. *Matlab Simulink solar PV module output results*

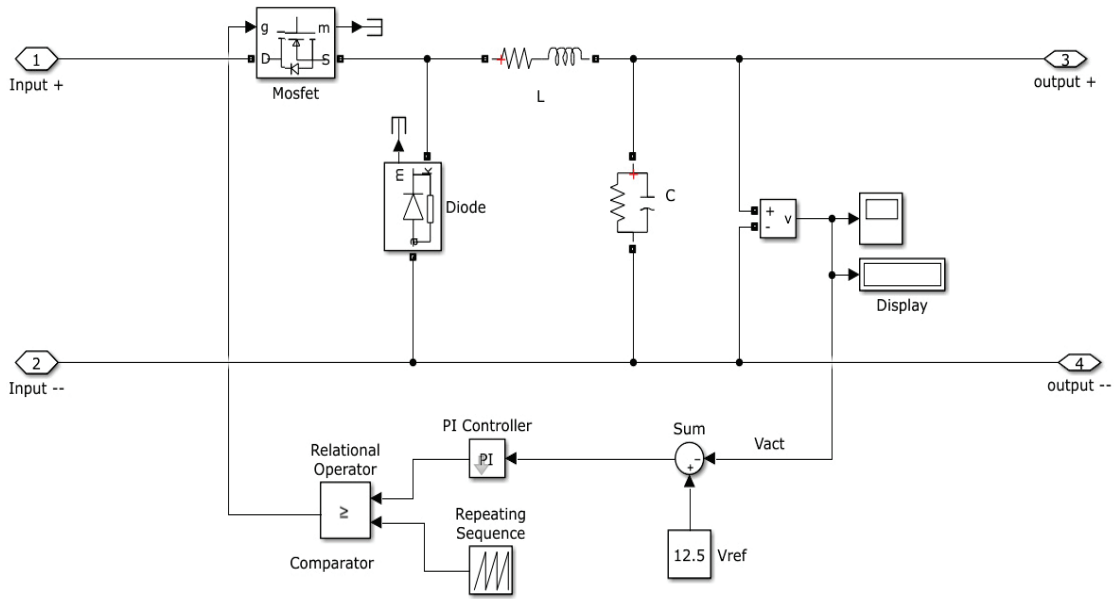

Fig. 9. *Matlab Simulink model of buck converter*

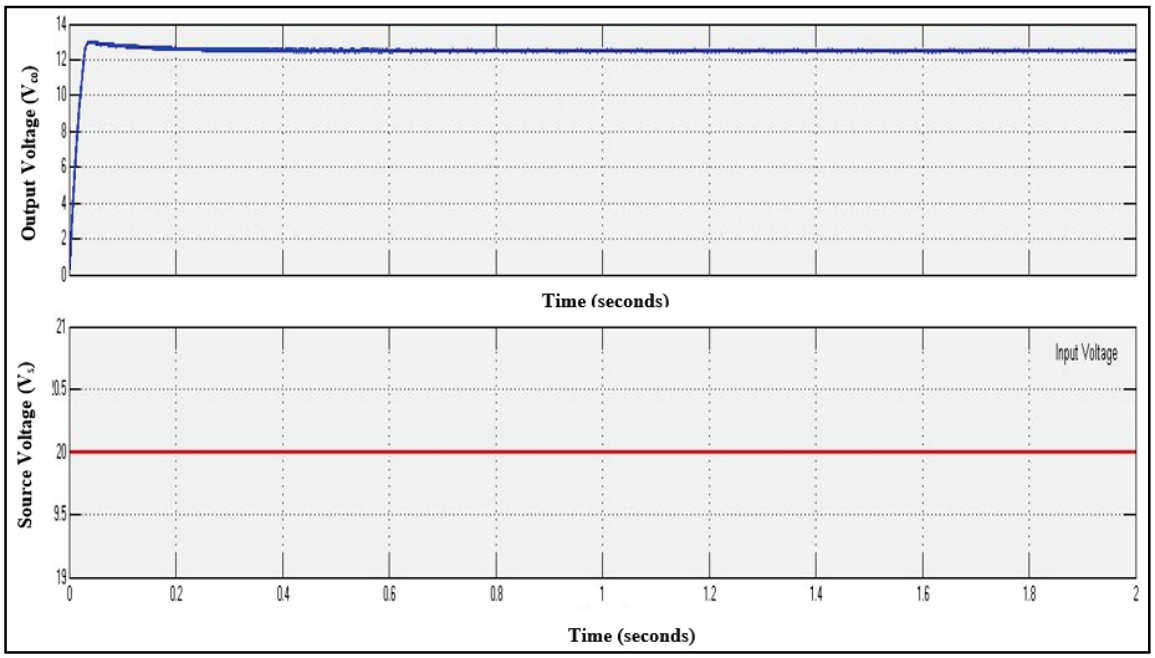

Fig. 10. *Converter output and input*

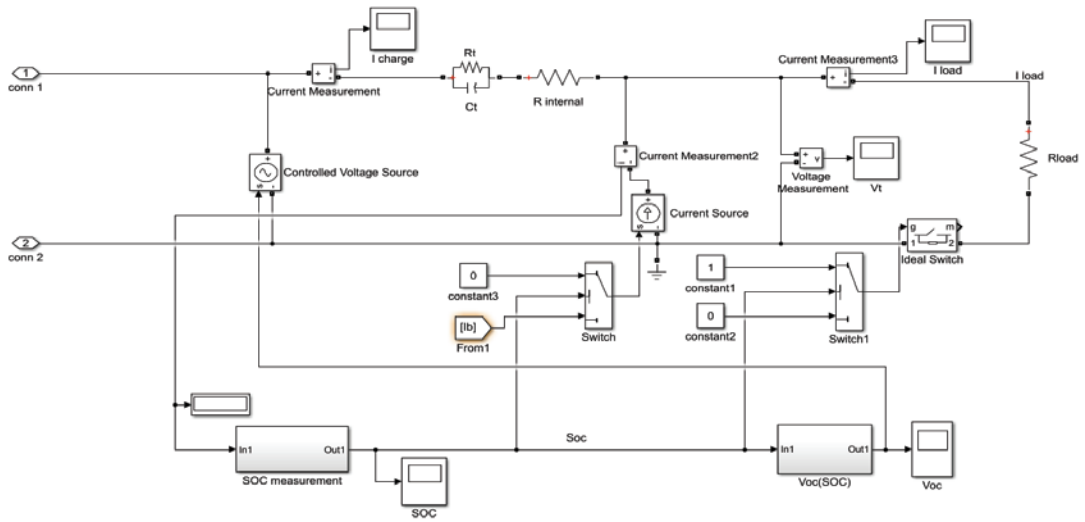

Fig. 11. *Matlab Simulink model of lithium polymer battery*

Depending on the SOC, two switches are used to connect or disconnect the load and source. When SOC>=1 (100 %), the load is connected and the source is disconnected, allowing discharge at a constant current up to a pre-set SOC level of 0.1 (10 %). When the battery SOC<=0.1 (10 %), the load is disconnected and the source is reconnected to charge the battery to its full capacity. The battery is charged and discharged at different C rates to obtain the dynamic characteristics of a lithium polymer battery used in low power applications. At a 100 % SOC, the battery voltage is 12.3 V.

6. Simulation results and discussions

As the battery open circuit voltage is a function of the SOC, i.e., $V_{oc1}=f\,[SOC]$, it was obtained experimentally using Equation (16). The graph in Fig. 12 shows the Matlab-simulated relation between V_{oc1} and SOC, from which it is seen that, at SOC=100 %, V_{oc1}=12.2 V, which is close to the maximum set cut-off voltage. When SOC = 10 %, V_{oc1} is close to 10.5 V, which is the minimum set cut-off voltage. When SOC = 9 % or below, *Voc* falls sharply below 10.5 V, resulting in over-discharging; for this reason, the lower SOC limit in this study was set to 10 %. Figure 12 shows the overall non-linear relationship between *Voc* and SOC.

Figure 13 shows a comparison of experimental and simulation results for a lithium polymer battery that is discharged across the load at a constant current rate of 0.96 C. It is seen that the experimental and simulated results are in close agreement.

Further simulations were conducted to obtain the discharge curves at different C rates to determine the corresponding dynamic behavior of the battery over one complete cycle (i.e., one complete charging and discharging of the battery). The battery discharge results at 0.2, 0.4, and 0.9 C are shown in Fig. 14, whereas the simulated dynamic behavior, SOC, and current through the battery over one cycle at 0.4, 0.9, and 1 C are shown in Figs. 15–17, respectively.

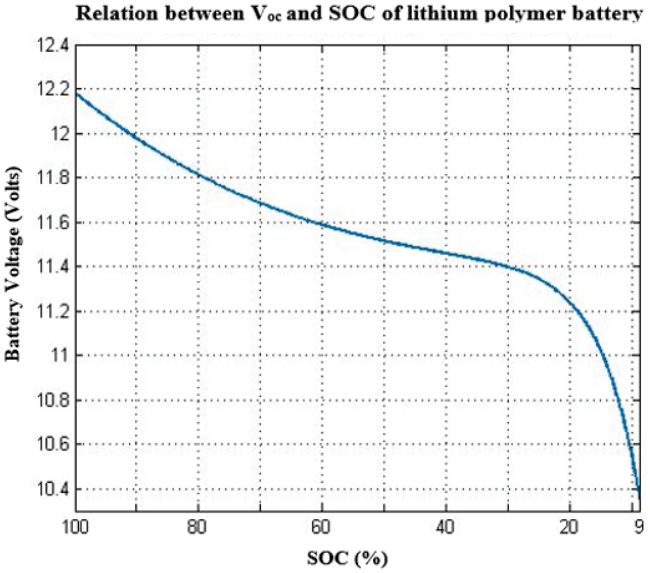

Fig. 12. *V_{oc1} as a function of SOC in lithium polymer battery*

In Fig. 15, which shows the 0.4 C case, it is seen that, starting from an initial state of discharge, at t=0 s the battery voltage (V_t)=10.6 V and SOC=0.05 (5 %), while the load current (I_L)=0 A. At t=0+s, charging commences at a constant charging current (*Ic*) of 2 A from the Solar PV module, causing V_t to build up as the battery SOC increases. At t=9,300s, V_t=12.25 V and SOC=1 (100 %). At this point, the controlling switch connects the load and disconnects the voltage source from the battery. At t=9,300+s, battery discharging commences at a constant discharging current (I_L) of 2.0 A across the load with *Ic*=0 A. At this point, V_t begins to decrease nonlinearly with respect to SOC. At t=18,300s, V_t=10.8 V and the SOC reaches its minimum cut-off level. At this point, the load is disconnected to avoid over-dis-

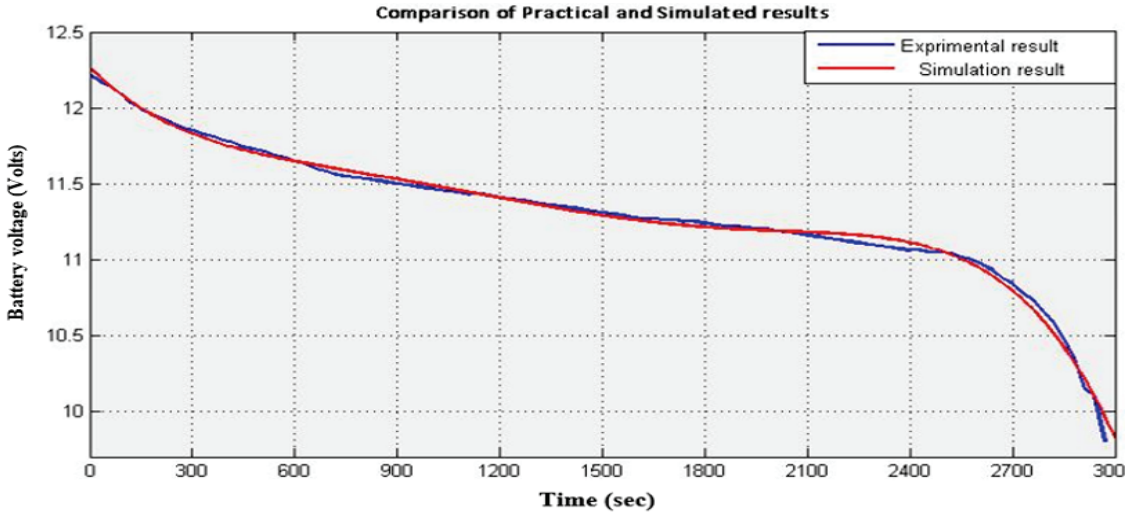

Fig. 13. *Experiment and simulation results*

charging. The total capacity C (Ah) achieved by the battery during charging can be obtained from Equation (10) as 5.17 Ah, which is very close to the rated capacity.

In the case shown in Fig. 16, the lithium polymer battery is charged by the solar PV module at 0.4C (2 A), while discharge is carried at a rate of 0.96C, i.e., 5.0 A. Although the charging behavior is similar to that in the earlier case, the dynamic behavior changes during discharge as a result of the high discharge rate. Increasing the discharge rate causes the capacity of the battery to fall at faster rate, which is evident from t=91,000 to t=12,300s. The non-linear relationship between battery voltage and SOC is maintained. Depending on how much the respective C rates differ, the maximum runtimes for charging and discharging diverge.

Figure 17 shows the results of charging at a rate of 1C (5.2 A), which is done using a Solar PV module with a higher power rating than under the 0.4 and 0.9C cases. In this case, continuous charging and discharging is carried out to obtain the dynamic behavior of the battery and predict the evolution of its SOC at 1C. It is seen from the figure that the maximum runtimes for charging and discharging over one cycle are very close. However, the source is disconnected at t=3,700 s when the SOC reaches one (100 %) and V_t=12.25V. After a rest period of a few seconds, the load is connected at t =3,800 s and the battery discharges at 5.2 A. At t=7,300 s, the SOC reaches 10 % and charging begins again after the load is disconnected.

It is evident from the above simulation results that lithium polymer has a sufficiently flat voltage profile

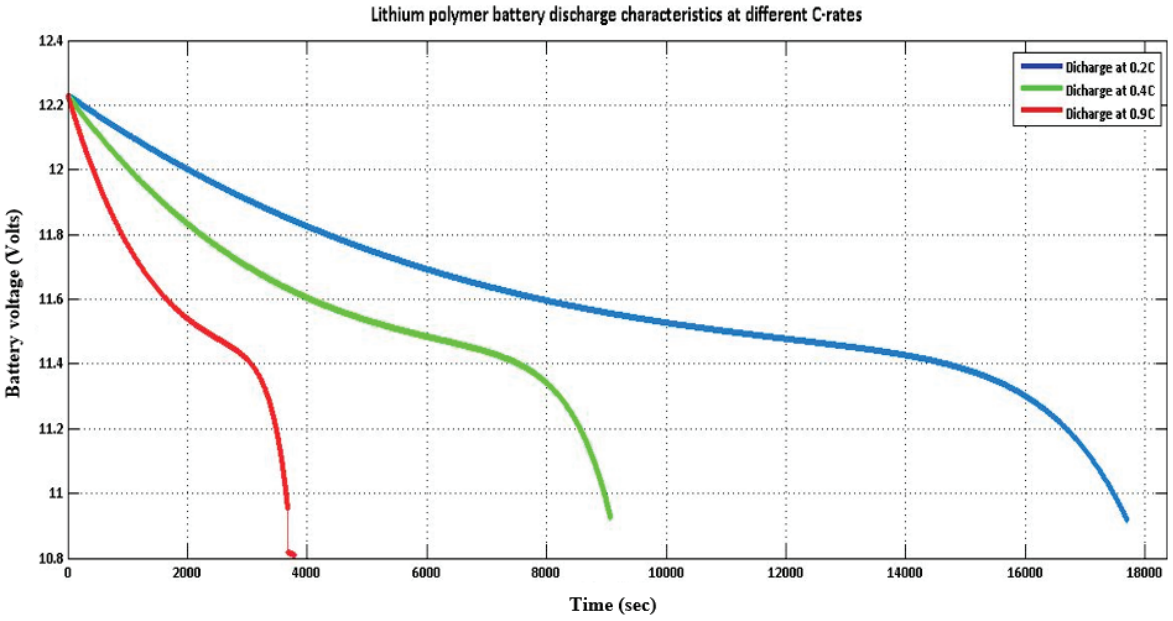

Fig. 14. *Discharge curves at different C rates*

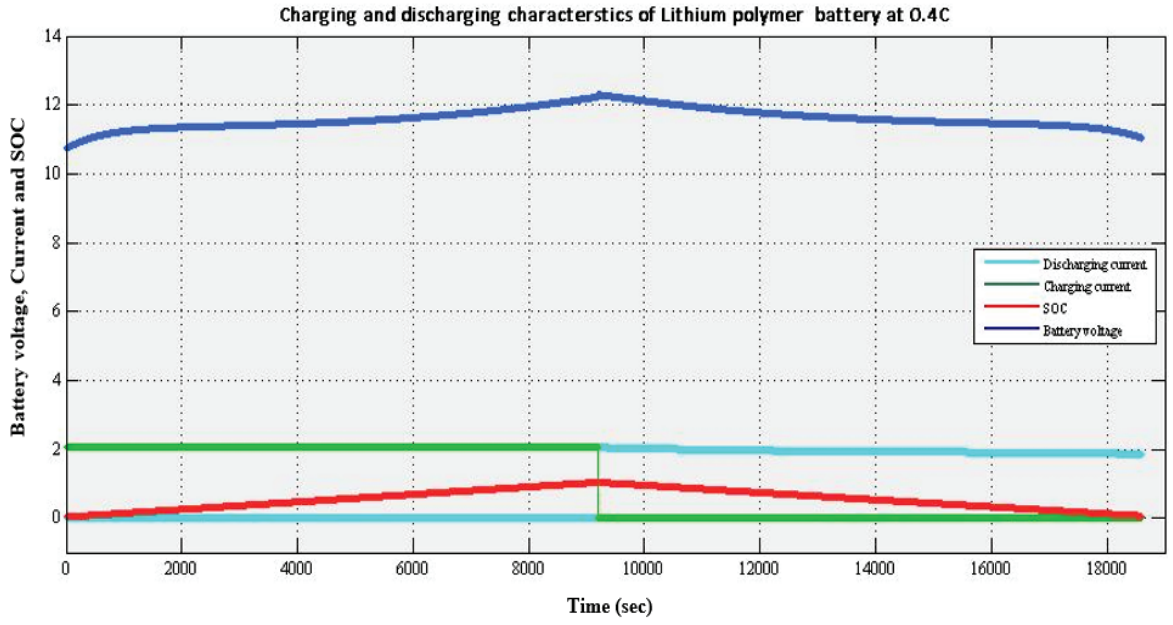

Fig. 15. *Lithium polymer battery dynamic behavior at 0.4C*

to supply a constant voltage to a load over long periods of time. As the C rates of charging and discharging increase, the capacity of the battery is reduced more rapidly; by contrast, the capacity is retained longer at small C rates. The battery can also be charged easily at up to a 1 C rate. The solar PV module was able to generate sufficient power to easily charge the battery at up to 0.5C rate.

7. Conclusion

In this study, a simplified model of a lithium polymer battery was used to capture the dynamic behavior of the battery. The model employs an electrical circuit model to forecast the dynamic characteristics of the battery, including the non-linear relation between V_{oc} and the battery SOC. A model for SOC tracking and runtime prediction was used to calculate the battery open circuit voltage. A simple experimental test procedure that could be rapidly executed was used to determine the electric parameters of the model. Simulation results confirmed the successful charging of the lithium polymer battery using Solar PV module. In addition to the battery, a Solar PV module and buck converter for charging the battery were also modeled. The model was able to capture the dynamic behavior of the battery during charging and discharging over a range of C rates. A comparison of the simulation results with experimental data confirmed the satisfactory response of the battery system model.

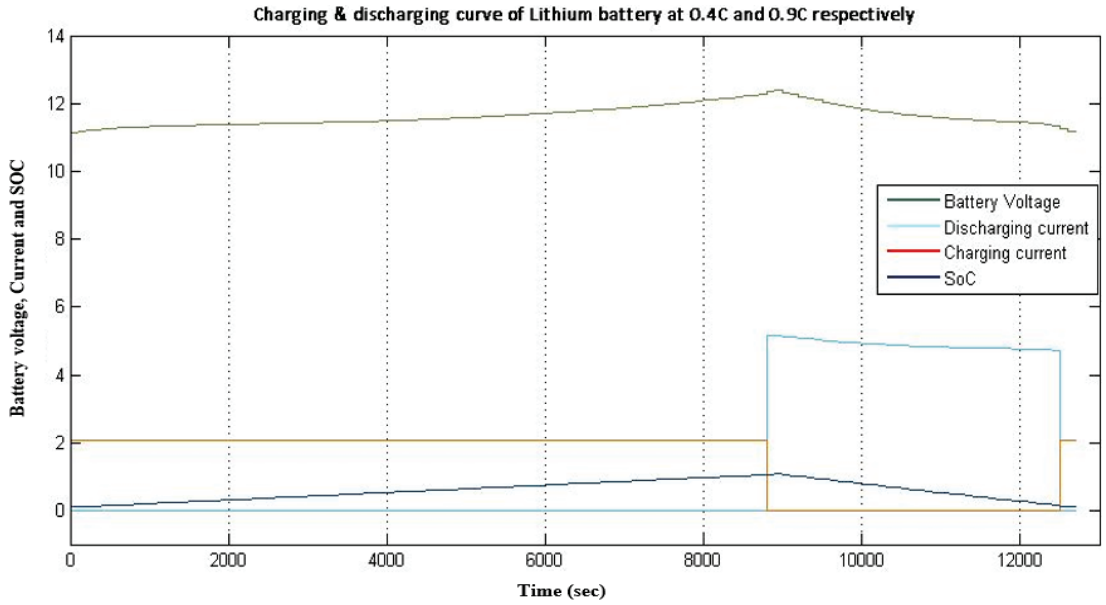

Fig. 16. *Lithium polymer battery dynamic behavior at different C rates*

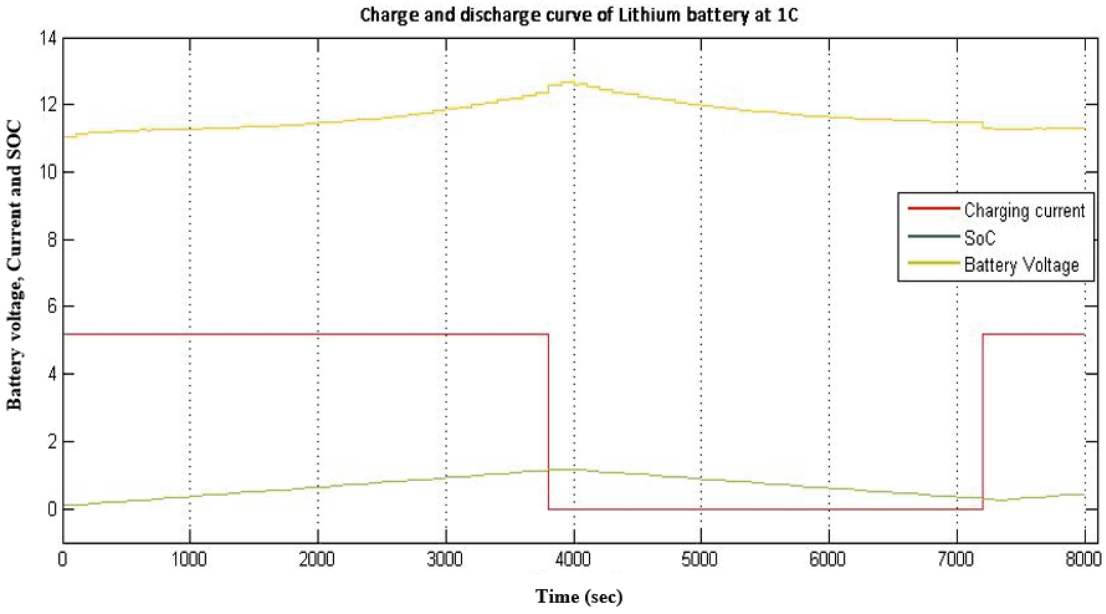

Fig. 17. *Lithium polymer battery dynamic behavior at 1 C*

Nomenclature

I_{rs}	Reverse saturation current
I_{ph}	Light generated current or photo current
I_o	Module saturation current
I_{pv}	Module output current
V_o	Module output voltage
T_{rK}	Reference temperature in Kelvin
T_{aK}	Module operating temperature in Kelvin
S	Solar Irradiance in W/m^2
q	Charge of electron ($1.6 \cdot 10^{-19}$ Coulomb)
A_i	Ideality factor
k	Boltzman constant ($1.3805 \cdot 10^{-23}$ J/K)
E_g	Silicon band gap (1.12 eV)
I_{scr}	Short circuit current at (25 °C & S=1000 W/m^2)
N_s	Number of cells in series
N_p	Number of cells in parallel
K_i	Short circuit coefficient at I_{scr}=0.00013 A/°C
R_s	Series resistance of module
R_p *or* R_{sh}	Parallel or shunt resistance of module
SOC	State of Charge
I	Current
V	Voltage
Ah	Ampere hour
V_t	Battery terminal voltage
V_t'	Battery terminal voltage just before relaxation begins
V_{oc1}	Battery open circuit voltage
R_t	Battery transient resistance
C_t	Battery transient capacitance
I_b	Battery current
R_i	Battery internal resistance
Hz	Hertz
Lipo	Lithium polymer

References

[1] World Energy Council. E-storage: Shifting from Cost to Value. Wind and Solar Applications. Available at: https://www.worldenergy.org/wp-content/uploads/2016/01/Resources-E-storage-2016.01.14_final__version.pdf

[2] Trends in Global CO_2 Emissions 2016 Report. Available at: http://edgar.jrc.ec.europa.eu/news_docs/jrc-2016-trends-in-global-co2-emissions-2016-report-103425.pdf

[3] Bashash S., Moura S.J., Forman J.C. and Fathy H.K. Plug-in hybrid electric vehicle charge pattern optimization for energy cost and battery longevity. *Journal of Power Sources,* 2011, vol. 196, no. 1, pp. 541–549. doi: 10.1016/j.jpowsour.2010.07.001.

[4] Rao V., Singhal G., Kumar A., and Navet N. Battery model for embedded systems. *Proceedings of the IEEE International Conference on VLSI Design*, February 2005, doi: 10.1109/ICVD.2005.61.

[5] Richardson D.B. Electric vehicles and the electric grid: A review of modeling approaches, Impacts, and renewable energy integration. *Renewable and Sustainable Energy Reviews*, 2013, vol. 19, pp. 247–254. doi: 10.1016/j.rser.2012.11.042.

[6] Tie S.F. and Tan C.W. A review of energy sources and energy management system in electric vehicles. *Renewable and Sustainable Energy Reviews*, 2013, vol. 20, pp. 82–102. doi: 10.1016/j.rser.2012.11.077.

[7] Dallinger D. and Wietschel M. Grid integration of intermittent renewable energy sources using price-responsive plug-in electric vehicles. *Renewable and Sustainable Energy Reviews*, 2012, vol. 16, no.5, pp. 3370–3382. doi: 10.1016/j.rser.2012.02.019.

[8] Mousavi S.M. An autonomous hybrid energy system of wind/tidal/micro- turbine/battery storage. *Int. J. Electr. Power Energy Syst.*, 2012, vol. 43, no.1, pp. 1144–1154. doi: 10.1016/j.ijepes.2012.05.060

[9] Kalantar M. and Mousavi S.M. Dynamic behavior of a stand-alone hybrid power generation system of wind turbine, microturbine, solar array and battery storage. *Applied Energy*, 2010, vol. 87, no.10, pp. 3051–3064. doi: 10.1016/j.apenergy.2010.02.019.

[10] Toledo O. M., Filho D.O. and Cardoso Diniz A.S.A. Distributed photovoltaic generation and energy storage systems: A review. *Renewable and Sustainable Energy Reviews*, 2010, vol. 14, no.1, pp. 506–511. doi: 10.1016/j.rser.2009.08.007.

[11] Rohit A.K., Devi K.P. and Rangnekar S. An overview of energy storage and its importance in Indian renewable energy sector: Part I–Technologies and Comparison. *Journal of Energy Storage*, 2017, vol. 13, pp. 10–23. doi: 10.1016/j.est.2017.06.005.

[12] Rohit A.K. and Rangnekar S. An overview of energy storage and its importance in Indian renewable energy sector: Part II–energy storage applications, benefits and market potential. *Journal of Energy Storage,* 2017, vol. 13, pp. 447–456. doi: 10.1016/j.est.2017.07.012.

[13] Lee Y.S. and Cheng M.W. Intelligent control battery equalization for series connected lithium-ion battery strings. *IEEE Trans. Ind. Electron*., 2005, vol. 52, no. 5, pp. 1297–1307. doi: 10.1109/TIE.2005.855673.

[14] Kim T. and Qiao W. A hybrid battery model capable of capturing dynamic circuit characteristics and nonlinear capacity effects. *IEEE Trans. Energy Conversion*, 2011, vol. 26, no. 4, pp. 1172–1180. doi: 10.1109/TEC.2011.2167014.

[15] Ishaque K. and Salam Z. An improved modeling method to determine the model parameters of photovoltaic (PV) modules using differential evolution (DE). *Solar Energy*, 2011, vol. 85, no.9, pp. 2349–2359. doi: 10.1016/j.solener.2011.06.025.

[16] Chen M. and Rincon-Mora G. A. Accurate electrical battery model capable of predicting runtime and IV performance. *IEEE transactions on Energy conversion*, 2006, vol. 21, no. 2, pp. 504–511. doi: 10.1109/TEC.2006.874229.

[17] Orioli A. and Di Gangi A. A procedure to calculate the five-parameter model of crystalline silicon photovoltaic

modules on the basis of the tabular performance data. *Applied Energy*, 2013, vol. 102, pp. 1160–1177. doi: 10.1016/j.apenergy.2012.06.036.

[18] Solanki C.S. *Solar Photovoltaic Fundamentals, Technologies and Applications,* 2nd Edition. New Delhi, PHI Learning Private Limited, 2011, 540 p.

[19] Rao R., Vrudhula S. and Rakhmatov D.N. Battery modeling for energy aware system design. *Computer*, 2003, vol. 36, no. 12, pp. 77–87. doi: 10.1109/MC.2003.1250886.

[20] Rohit A.K., Tomar A., Kumar A. and Rangnekar S. Virtual lab based real-time data acquisition, measurement and monitoring platform for solar photovoltaic module. *Resource-Efficient Technologies*, 2017, vol. 3, no. 4, pp. 446–451. doi: 10.1016/j.reffit.2017.04.006.

[21] Agarwal V., Uthaichana K., DeCarlo R.A. and Tsoukalas L.H. Development and validation of a battery model useful for discharging and charging power control and lifetime estimation. *IEEE Transactions on Energy Conversion*, 2010, vol. 25, no. 3, pp. 821–835. doi: 10.1109/TEC.2010.2043106.

Received 30.06.2018